Illicit Material Detection using Dual-Energy X-Ray Images

Reza Hassanpour

Computer Engineering Department, Cankaya University, Turkey

Abstract: *Dual energy X-ray inspection systems are widely used in security and controlling systems. The performance of these systems however, degrades with the poor performance of human operators. Computer vision based systems are of vital importance in improving the detection rate of illicit materials, while keeping false alarms at a reasonably low level. In this study, a novel method is proposed for detecting material overlapping and reconstructing multiple images by alleviating these overlaps. Evaluation tests were conducted on images taken from luggage inspection X-ray screening devices used in shopping centres. The experimental results indicate that the reconstructed images are much easier to inspect by human operators than the unprocessed original images.*

1. Introduction

Aviation security, the control of drug trafficking and baggage inspection in public places such as shopping malls, has mainly relied on X-ray screening technology [6, 22]. The screening process is subject to error due to the screeners missing of potentially dangerous objects. The degradation in the performance of staff can be due to many different factors of which the most important are a large turnover of unexperienced staff and the repetitive nature of the work. The inspection devices generate many false alarms that require human intervention. In addition, the large number of passengers at airports makes it impossible to check every bag [2]. These factors clearly demonstrate the need for an automatic alert system based on computerized processing of the X-ray images. A major drawback of the existing dual-band X-ray systems can be solved if a complete 3D scan of the luggage is provided. These types of imaging systems are very similar in their technology to the Computed Tomography (CT) imaging systems used in medical examinations. The main disadvantage of these systems is the long exposure of the objects being examined to X-ray radiation. Hence, illicit materials hidden under clothes will not be detected by these systems. Besides, the processing time of these systems is undesirably long. Moreover, X-ray screening systems are based on measuring the attenuation of the signal imposed by the material through which it is sent. The detectors can measure the total attenuation regardless of the overlapped materials. This means thin materials with low-density, hidden behind a thick or high-density material, can remain undetected during the inspection process. Solutions based on technologies such as z-backscatter or thermal neutron are not commonly accepted, either due to their high cost or threats to human health. In this study, an image processing based method for reducing the effect of overlapping in dual energy X-ray images is introduced. Some authors have tried to replace the explosive detection methods which rely on X-ray image post-processing, with methods based on the physical characteristics of explosives. Pfeiffer *et al.* [21] enhance the yield dark-field scatter images to a higher quality by an approach based on a grating interferometer, which they claim can be used with conventional X-ray tube sources. They higher contrast is formed through small-angle scattering and provides complementary structural information. Pramanik *et al.* [23] claim the unique selectivity of some material can be used for the detection of high explosives through a fluorescence quenching and enhancement mechanism. Lan *et al.* [13] demonstrate that some highly luminescent microporous metal-organic frameworks are capable of detecting explosives.

In the following sections we compare dual energy X-ray imaging technology with single energy X-ray, scattering detection and thermal neutron technologies. Then, we introduce our proposed method followed by the experimental results.

2. Screening Technology

The X-ray based inspection of luggage is carried out by means of interpreting the images using the physical properties of the X-ray signal's interaction with the materials. Theoretically, X-ray images can be used for determining the density and effective atomic number of the materials. By density we mean the amount of mass per unit volume through which the signal passes. Generally the materials inspected are not made of a single element; hence the attenuation caused is the result of the interaction between a compound matter and the X-ray signal. Therefore, effective atomic number is more suitably used to describe these

materials. Effective atomic number Z_{eff} is defined as the atomic number of a hypothetical matter which behaves the same as the compound matter being inspected [4]. Figure 1 depicts the relative values of Z_{eff} versus density for organic, inorganic, drugs and explosives. Conventional X-ray devices measure signal attenuation after it has passed through a scanned object [10].
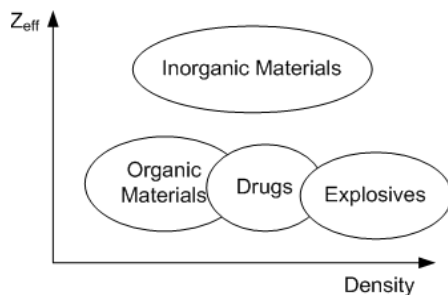

Figure 1. Effective atomic number versus density in X-ray scanning image.

This equipment has a fan shaped X-ray beam whose absorption is measured by a line of detectors. These measurements are used in producing an intensity image where each pixel value corresponds to the amount of absorption by the scanned object. As the resultant attenuation is the total absorbtion by the materials between the X-ray beam source and the detectors, a thin strong absorber cannot be distinguished from a thick but weak absorber [19]. Kravis [11] utilizes THz (far-infrared) for explosive detection. The main advantage of these waves is that they can penetrate through many dielectric materials such as paper, textile, and plastic, they have low photon energy (4 meV for 1THz) and are not harmful. The authors tested their method on a solid-state explosive named RDX (hexahydro-trinitro-triazine), which measures reflection spectrum of the explosive RDX from a diffuse reflection using a THz time-domain spectroscopy. The authors report small spectral variations in the absorption spectra of polyethylene and flour which differs from the transmission measurements of polyethylene. They attribute the difference to the surface selection rule which is the result of a phase shift in the THz waves that occurs upon reflection. Although, the reflection spectra are reported to distinguish RDX from other martial, the water vapor absorption almost attenuates the THz signal and creates artificial spikes.

2.1. Dual Energy X-Ray Imaging

X-ray signal attenuation is a function of the density of the material being inspected. Therefore, to detect materials with higher density, such as weapons, higher energy levels of over 100 keV, are used. In these images dense objects such as weapons appear as dark regions. However, less dense objects such as organic materials (for example drugs) placed behind denser materials are not detected. In low energy levels, below 80 keV, the energy absorbtion is a function of effective atomic number. Therefore, materials with low-density,

hidden behind a high-density material, will further reduce the signal energy [12]. This means that while the areas corresponding to metal are dark in both images, a low-density object behind a high-density metal can be detected by comparing low and high-energy images. A system that uses two X-ray energy levels is called a dual-energy imaging system [4]. Kravis [11] tries to solve the CT scanning problem by performing a post-processing on the X-ray images. The output of the post-processing stage provides the potential locations of the illicit materials (explosives in this case). At the next step, they perform a more detailed scanning by changing the X-ray beam source direction and capturing images from different angles. The main advantage of their proposed method is reducing the exposure time to X-ray of the objects being inspected by determining the suspicious areas through a post-processing stage. However, overlaying objects with different average atomic numbers can make theses detections difficult. Moreover, since the X-ray beam angle change is limited, the new images may fail to provide new information.

2.2. Back Scattering

An X-ray signal on interaction with the material is either absorbed, penetrates the matter, or is reflected as a scattered signal [15]. Transmission X-ray images are obtained from the signal that penetrates the matter, whereas back scatter images are obtained from a signal that is scattered back towards the X-ray source. A set of detectors beside the X-ray beam source measure the scattered signal, and an image is created. This scattering effect is known as compton scattering [1]. Objects with greater density or higher Z_{eff}, block or absorb X-ray signals more than objects with lesser density. This means materials with higher Z_{eff} are more likely to absorb X-rays, while materials with a lower Z_{eff} scatter the signal more strongly. Hence, the method is referred to as z-backscatter screening [3]. Many organic materials are low-density, and do not appear well on traditional transmission X-ray images. Organic materials, such as explosives and drugs, contain low atomic number elements such as carbon, oxygen, hydrogen and nitrogen. These materials are clearly visible in backscattered images.

2.3. Thermal Neutron based Screening

The main idea behind Thermal Neutral Analysis (TNA) is measuring gamma rays emitted from the nucleus of the materials being inspected. A radioactive source is used to generate a thermal neutron beam. The neutrons striking the nucleus of the materials are absorbed with a certain probability. Then, gamma rays are emitted from the nucleus with an energy that depends on the characteristics of the atom [7]. The analysis of the emitted gamma rays helps in identifying certain elements such as nitrogen which is used in explosives (trinitrotoluene $C_7H_5N_3O_6$ or pentaerythritol tetranitrate $C_5H_8N_4O_{12}$ for instance). However, current TNA devices have limited capability to detect oxygen

or carbon, although hydrogen, chlorine and some other elements are detected [26]. This restriction results in a high rate of false alarms from nitrogen present in other materials. In addition, their highly expensive price has a prohibitive impact on their widespread usage.

3. Processing Inspection Images

Runkle *et al.* [25] discuss aviation security screening systems including image processing based methods. Manukian *et al.* [18] use AS and E 101 X-ray images for drug detection. The images provided as input are backscatter and transmission X-ray images, in which the outlines of the suspicious regions have been marked. They use two neural networks to analyze the combination of both backscatter and transmission data. They use the first network to analyze suspicious regions from the images and the second network to integrate all such regions to output a probability of the existence of drugs.

Harding [5] reports a method for combining the results of a compton backscatter X-ray with an X-ray tomography imaging system for explosive detection. By examining the energy-dispersive diffraction profiles of different materials, and comparing them with the profiles obtained from explosives, they try to detect explosives. In the research work carried out by Lu and Conner [16, 17] both the dual energy X-ray and the backscatter technologies are used for acquiring images. They have defined two distinguishing features that are based on a material's Z_{eff} value, and its density. To reliably calculate these quantities from the images they use the intensity value measured for air where no background object is present and use it as reference point for the remaining intensity values.

Liu and Chen [14] tried to detect elongated objects such as detonators using Gabor filters and Hough transform. He then fuses the information from Gabor filters and hough transform and uses the size of the detonator by considering its orientation in the image.

Yang *et al.* [27] use dual energy X-ray images together with neutron induced information to find explosives concealed in cargos. More specifically, they try to detect explosives shielded by metal or other organic materials. Using a high energy X-ray induced photoneutron analysis, they obtain the 2-dimensional elemental distribution of hydrogen, nitrogen and iron. Then, they mark areas high in nitrogen and hydrogen which are suspected to be explosives. They noticed that areas of organic materials could be first notified effectively by dual energy imaging, then the 2-dimensional element information of nitrogen and hydrogen can be used to confirm the existence of explosives. Ipe *et al.* [8] report similar studies where X-ray imaging and thermal neutron inspection are used for explosive and drug detection in airport cargos. Ipe *et al.* [9] also, considered pulsed fast thermal neutron analysis for cargo inspection.

The main disadvantage of the thermal neutron based inspection methods is that fast high-energy neutrons create a significant background in gamma ray detectors which deteriorates the extracted information. Meanwhile, developing a practical neutron beam with safe, cost effective, and operationally acceptable characteristics is difficult. The distinguishing feature of the proposed method is its reliance on well understood and commonly used dual energy X-ray screening systems.

4. Proposed Method

To overcome the overlapping problem in dual energy X-ray images a multi-layer processing method is proposed. The proposed method assumes a limited number of layers corresponding to metal, organic and inorganic materials in different thicknesses, which can occur in the X-ray images. The main goal of the proposed method is to generate a set of images corresponding to each layer by using the intensity values of the pixels, and to estimate and compensate for the overlapping regions. As an initial step, the proposed method applies an edge preserving smoothing filter to the images for noise removal. Next, the image is segmented into sub-regions based on the intensity level similarity of the pixels. Then, an overlapping detection algorithm is developed for estimating the regions that belong to each intensity layer, and generating the corresponding images. The following sub-sections explain each step in details.

4.1. Smoothing

The imaging artifacts such as noise affect the uniformity of the intensity values of a region. These non-uniformities are of no importance from the information content perspective. A smoothing process can greatly improve the results of segmentation and boundary detection steps, by reducing these kinds of non-uniformities in the object regions while preserving edges. In this study, an anisotropic linear diffusion filter is used for smoothing the images. The isotropic linear diffusion for an image I is given by [20]:

$$\frac{\partial I}{\partial t} = \nabla c . \nabla I + c \Delta I \quad with \quad c = e^{-|\nabla I|^2 / k^2} \qquad (1)$$

Where the conductivity coefficient c makes the diffusion adaptive to local image structures and k is a constant.

4.2. Histogram Analysis and Thresholding

Each region, with almost similar intensity valued pixels, corresponds to a peak point in the intensity histogram of the image. These peak points are approximately equal to average intensity values of the regions, and hence are used as seed points for their region growing based segmentation. To avoid having local maxima accepted as histogram peak points, histogram smoothing is applied. A running window of size 7 is used for averaging over the histogram bins. Let the original histogram be defined as $H=\{h_i\}$ for $i=0, 1, ..., L$. Then, the smoothed histogram is defined as:

$$H^s = \{h_i^s\} \quad for \quad i = 0, 1, ..., L \tag{2}$$

Where as $h_i^s = \dfrac{1}{w} \sum\limits_{j=i-w/2}^{i+w/e} h_j$. And w is the running window size, which here is selected as 7. Figure 2 depicts the intensity distribution histogram of the x-ray image of Figure 3-a after smoothing.
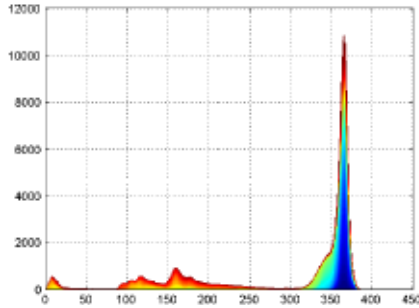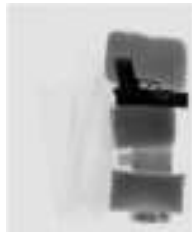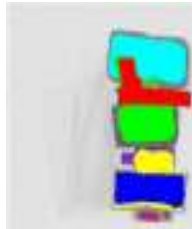

Figure 2. Intensity distribution histogram.

a) Sample X-ray scanning image containing organic, inorganic and metallic objects.

b) Result of segmentation using region growing.

Figure 3. Results of segmentation using region growing.

4.3. Region Growing

A 7×7 window is slid over the image. Whenever, all pixels falling under the window are equal to one of the peak values of the histogram, within a range of a threshold, then the center of the window is selected as a seed point for region growing. Regions finally coalesce at the end of the segmentation process. This procedure is performed in both low and high-energy images. For each region a feature vector is defined using the seed point intensity value, the average intensity of the region in low and high-energy images, and the average intensity difference between the low and high-energy image for that region. This vector is stored as the characteristic feature vector of the region. Figure 3 depicts a sample X-ray scanning image and the result of applying the segmentation algorithm to it.

A morphological opening, followed by morphological closing operations, is used for eliminating thin connections between the segmented regions. This step has not been shown in Figure 3.

4.4. Multi-layer Processing

The segmented regions are further processed for estimating the overlapping areas and compensating for them. In both low energy and high-energy images, the attenuation coefficient along any direction is a function of the amount of energy absorbtion by all material along that direction.

The attenuation coefficient expressed in decibels however, is the sum of the attenuation coefficients of each material absorbing signal energy, along the given direction, as indicated in Equation 3.

$$\Gamma = \sum_i \alpha_i \quad where \quad \alpha_i = 10 \log \frac{I_i^{in}}{I_i^{out}} \tag{3}$$

This characteristic of signal absorbtion is used for estimating the overlapping areas in the images. For each segmented region, the attenuation coefficient is computed using the average intensity values. The regions are then labeled using these attenuation coefficients as depicted in Figure 4 which also displays some of the possible overlapping cases.

Case 1   Case 2
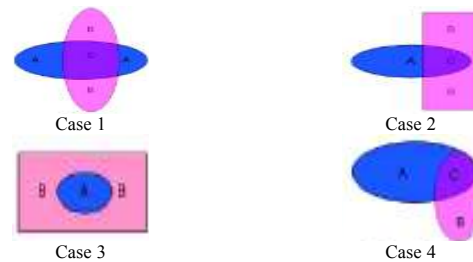
Case 3   Case 4

Figure 4. Possible overlapping cases labeled using their attenuation coefficients.

In the overlapping cases indicated by cases 1, 2, and 4 in Figure 4, the area in the middle (labeled as C) has an attenuation coefficient equal to the sum of the adjacent areas attenuations (areas labeled as A and B). This means that if we subtract the attenuation coefficient value of one the adjacent areas from the attenuation coefficient value of the area at the middle, we can reconstruct the region after removing the overlapped region. This can be seen in case 1 in Figure 4, where the horizontal elliptical area is reconstructed by subtracting the attenuation coefficient of region B from region C. In case 3 the larger region completely overlaps the smaller region. To remove the overlapping, and reconstruct the regions, the background is considered as a distinct region. Hence, if a region has only one adjacent region (which is not the background region) and its attenuation coefficient is larger than its adjacent region then case 3 is assumed.

Meanwhile, for each region a characteristic label ξ is computed by finding the weighted sum of the components of its feature vector. The weight values have been selected to be 0.2, 0.2, 0.2, 0.4 empirically. This weighted sum emphasizes the Z_{eff} value by giving a weight coefficient of 0.4 to it and considers equal

importance for the remaining features. Algorithm 1 is used to create a layer image:

Algorithm 1: Create layer image(G).

foreach(Region R_C)
    foreach(R_i and R_j in Nc)
        if (I_c - $|I_i+I_j|<\epsilon$)
          {
            if(R_k in Nc and $\xi_k = \xi_i$ and $I_k=I_i$)
             {
               $G(C1, area)= Merge(R_i, R_k, R_c)$
               $G(C1, intensity)=I_i$
             }
            else if($\xi_i = \xi_c$ - ξ_j)
              {
                 $G(C2, area)= Merge(R_i, R_c)$
                 $G(C2, intensity)=I_j$
              }
          else
            {
              $G(C1, area)= R_c$
              $G(C1, intensity)=I_i$
              $G(C2, area)= R_c$
              $G(C2, intensity)=I_j$
            }
          }
        else if(R_i in Nc and $N_i=R_i$)
        {
          $G(C1, area)= R_i$
          $G(C1, intensity)=I_i$- I_c
          $G(C2, area)= Merge(R_i, R_c)$
          $G(C2, intensity)=I_c$
        }

return G

Where R_a refers to region *a*, N_c is the set of neighboring regions around *C*, I_a is the attenuation coefficient of region *a* and ε_T is a threshold value.

To represent the regions and their adjacency to one another, a bidirectional graph is used. The background is also modeled as a region. The adjacency graph is implemented using an adjacency matrix for faster and easier search.

5. Experimental Results

The proposed algorithm is tested against a set of more than 120 dual energy X-ray images taken using a rapiscan 618XR X-ray screening system. The images are taken from materials having different Z_{eff} values including the values close to explosives and narcotics. Figure 5 show an example of our data set.

Figure 5. Sample test data: Metal and organic material overlap.

For organic materials we considered flour and sugar. Sugar shows very similar properties to heroin under X-ray screening. Sugar with molecular formula $C_{12}H_{22}O_{11}$ has a Z_{eff} value of about 7.1 while cocaine ($C_{17}H_{21}NO_4$) and heroin ($C_{21}H_{23}NO_5$) have Z_{eff} values of 9.1 and 8.9 respectively. Sugar, cocaine, and heroin have very close density value of about 1.1g/cm^3 and for practical purposes, sugar is different only in a missing nitrogen atom. To examine the properties of inorganic materials we used salt. Inorganic and organic materials show very different characteristics in low and high power X-ray images, as indicated in section 2.1. However, when these two different materials overlap, many screening systems are unable to classify them as either organic or inorganic materials. In Figure 6-a the X-ray image of a pack of sugar under a pack of salt is shown. However, because of incomplete overlapping, the adjacency graph of the segmented regions shows neighboring regions with lower attenuations for the overlapped area. Figures 6-b and c depict the results of applying the proposed algorithm to create multi-layer images. In the middle image, removing the impact of attenuation given by inorganic material has exposed organic material, while in the Figures 6-c, inorganic material has been exposed. An important point to consider is the existence of thin areas around the packages where attenuation is low due to lower material thickness. The post-processing to be applied to these images for shape analysis, should consider this characteristic of the output images.

a) Original image.   b) Organic material exposed.
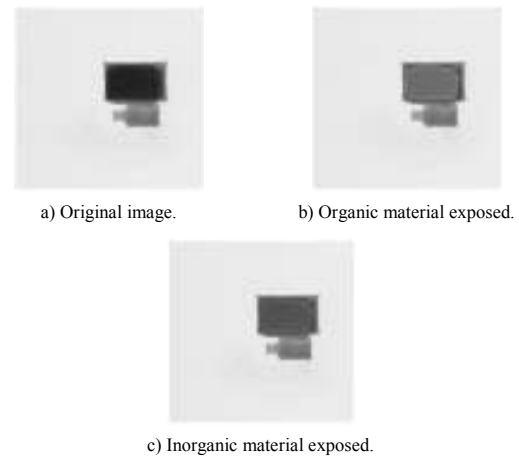
c) Inorganic material exposed.

Figure 6. Organic and inorganic material overlapping.

Figure 7 depicts the result of applying the proposed method to the sample image of Figure 3-a. The metallic gun overlaps the organic materials whereas, part of it does not overlap with any other material. It is important to note that the gun does not have a uniform thickness and hence the attenuation values at its different parts are not the same. This difference in thickness is the main reason behind the thin edges belonging to the gun shown in the reconstructed image. To evaluate the performance of the method numerically, we manually segmented and labeled the objects in the input images. The notation used for labeling, assigns a digit label to objects which do not overlap any other object. For the overlapping objects, the numeric label of the object on the top is multiplied

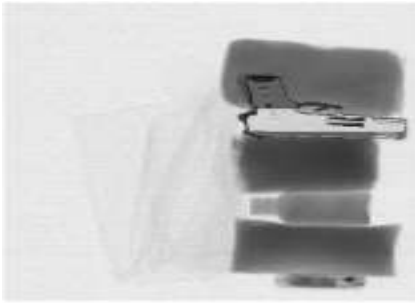by 10 and added to the the numeric label of the object under it.

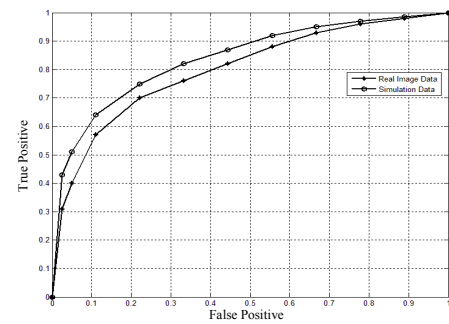Figure 7. Remove overlapping metallic material.

In case of three objects overlapping each other (three layers), the topmost object's label is multiplied by 100, the middle object by 10, and then these labels are added to the numeric label of the object at the bottom. In our experimental images, we have no case of four or more overlapping objects. It is important to note that the non-overlapping parts of the objects preserve their label. This notation helps us to develop an algorithm to count the number of labels marked as overlapping regions, and their respective relationships with their neighboring regions. The rate of false recognitions and true recognitions in all test images is 14.3% and 67.6% respectively. These rates are obtained by considering the number of regions recognized incorrectly (false recognition)/correctly (true recognition) divided by the total number of regions in each image respectively. Then, the average rates on all images have been computed. The true recognition includes detecting non-overlapping regions, detecting overlapping regions, and detecting the non-overlapping parts of the objects contributing to the overlapping region. False recognition cases include considering an overlapping area as non-overlapping and vice versa and error in detecting the object areas which contribute to a detected overlapping region.

An important effective factor in detecting the overlapping areas is determining the threshold values. Since, many objects are thinner close to their boundaries, the attenuation becomes less and hence the corresponding areas are not counted as part of the object. On the other hand, considering a larger range for a matrail/object results in a higher false positive rate. The range of The pixels from the manually segmented and labeled areas are used to verify the accuracy of the proposed method with different thresholding ranges using ROC curves. In addition, the result of applying the method on simulation data is compared to the results from the test images. In generating simulation data, for each material we have considered an average attenuation value and a standard deviation. The area belonging to the object is filled in by generating random values in the given range for that material. We also, gradually reduced the threshold value at the boundaries of the object. Three cases have
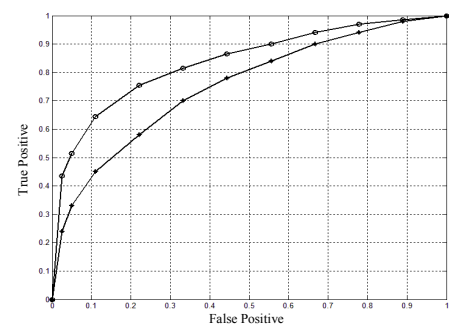
been considered where the overlapping is created with metal+organic material, metal+inorganic material, organic material+inorganic material. ROC curves depicted in Figure 8 compares simulation data results with real image data for each case.
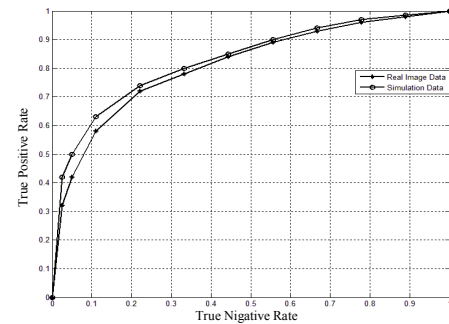
a) Overlapping metal and organic material.

b) Overlapping metal and inorganic material.

c) Overlapping organic and inorganic material.

Figure 8. ROC curve.

Although, standard deviation defines the range of differences with the threshold value of each material, random noisy points can fall out of the range in real images. This is the main reason for faster convergence in simulation data. Secondly, both real and simulation data indicate that overlapping organic and inorganic material is hard to detect compared to the overlapping with metals. First of all, metal objects are man made and have more uniform shapes and thicknesses. This makes detecting their boundaries easier. Second, the attenuation rate difference between metal objects and organic/inorganic objects is relatively high. Hence, the pixels from one material type do not fall in the range of the other material. Besides, a close examination of the results shows that most of the failed cases belong to one of the following two groups:

1. The overlapping objects are from the same group of objects. For instance, when a pack of flour and a

pack of sugar overlapped, the algorithm detected the overlapping area but since, the attenuation rate of non-overlapping parts of sugar and flour were very close, the algorithm decided it as case 3 while the true result was case 1 as shown in Figure 4.

2. The overlapping object completely hides the underneath object. The algorithm assumes them as a single object.

At a failure rate of 14.3%, the algorithm shows a 67.6% rate of success. It is worth to note that, the results reported here are related to the experiments where the algorithm chooses an overlapping case which seems more probable. Considering the sensitivity of the application, a reasonable rate of false alarms are tolerated although, amny methods reported in the litearture canbe used to reduce this rate [24]. Besides, in many experiments, two or more cases were among the possible solutions. We believe that a semi-automatic implementation where the system displays possible reconstructions with a minor user interaction can greatly improve the performance.

7. Conclusions

An algorithm for alleviating overlaps in dual energy X-ray images is proposed. The main idea behind the proposed method is that the intensity values of the pixels are the result of signal attenuation given by the materials on the signal path. Since, the total attenuation expressed in dB is a linear sum of the attenuations imposed by each material along the signal path. Analyzing the images as segments with equal attenuations and considering the adjacency of these segments are used to estimate the type of overlapping materials and reconstruct the images in multi-layers. The experimental results indicate that the proposed method can be used for improving the automatic shape analysis and illicit material detection systems. Our experiments show a good success rate with low false responses. On the other hand, the proposed algorithm can be used with much higher performance if applied to a semi-automatic system and used together with a human operator. A main drawback of the two-dimentional imaging systems is their lack of providing any volume information about the objects being inspected. A reliable detection of contraband matrials such explosives, narcotics, and weaponry can be reliably done through a three-dimentional scanning of the luggages. Segmentation algorithms are applicable in these cases in combination with the a-priori knowledge from the environment, and fusing data from other sources. Meanwhile, the results of this research will benefit the scientific and research community by providing information on subjects which has been considered proprietary.

References

[1] Arendtsz N. and Hussein E., "Compton Scattering for Density Imaging," *IEEE Transactions on Nuclear Science*, vol. 42, no. 6, pp. 2155-2165, 1995

[2] AS&E., "Technology for Combating Illegal Drugs and Terrorism," *American Science and Engineering*, Annual Report, 1996.

[3] Chen S., Avakian H., Burkert V., Vandenaweele L., and Eugenio P., "Measurement of Deeply Virtual Compton Scattering with a Polarized Proton Target," *Physical Review Letters*, available at: http://arxiv.org/pdf/hep-ex/0605012.pdf, last visited, 2006.

[4] Eilbert R. and Krug K., "Aspects of Image Recognition in Vivid Technology's Dual-Energy X-Ray System for Explosive Detection," *in Proceedings of SPIE 1824*, pp. 127-143, 1992.

[5] Harding G., "X-Ray Scatter Tomography for Explosives Detection," *Radiation Physics and Chemistry* vol. 71, no. 3-4, pp. 869-881, 2004.

[6] Haupt S., Rowshan S., and Sauntry W., "Applicability of Portable Explosive Detection Devices in Transit Environments," available at: http://www.worldtransitresearch.info/research/3030/, last visited 2004.

[7] Hussein E., "Detection of Explosive Materials Using Nuclear Radiation: A Critical Review," *in Proceedings of SPIE 1736*, pp. 130-137, 1992.

[8] Ipe N., Akery A., Ryge P., Brown D., Liu F., Thieu J., and James B., "An Airport Cargo Inspection System based on X-Ray and Thermal Neutron Analysis (TNA)," *Radiation Protection Dosimetry*, vol. 116, no. 1-4, pp. 347-351, 2005.

[9] Ipe N., Olsher R., Ryge P., Mrozack J., and Thieu J., "A Cargo Inspection System based on Pulsed Fast Neutron Analysis (PFNA)," *Radiation Protection Dosimetry*, vol. 116, no. 1-4, pp. 343-346, 2005.

[10] Kramers H., "On the Theory of X-ray Absorption and of the Continuous X-ray Spectrum," *Philosophical Magazine Series 6*, vol. 46, no. 275, pp. 836-871, 1923.

[11] Kravis S., "X-RAY Inspection System for Detecting Explosives and other Contraband," *available at*: http://www.google.com/patents/US7092485, last visited 2006.

[12] Krug K. and Stein J., "Advanced Dual Energy X-Ray for Explosives Detection," *in Proceedings of the 1st International Symposium on Explosive Detection Technology*, pp. 282-284, 1991.

[13] Lan A., Li K., Wu H., Olson D., Emge T., Ki W., Hong M., and Li J., "A Luminescent Microporous Metal-Organic Framework for the Fast and Reversible Detection of High Explosives," *Angewandte Chemie International Edition*, vol. 48, no. 13, pp. 2334-2338, 2009.

[14] Liu H., and Chen Y., Bastiaans G., and Zhang X., "Detection and Identification of Explosive RDX by THz Diffuse Reflection Spectroscopy,"

Journal of Optics Express, vol. 14, no. 1, pp. 415-423, 2006.

[15] Liu W., "Automatic Detection of Elongated Objects in X-ray Images of Luggage," *Master's Thesis, Department of Electrical and Computer Engineering, Virginia Tech. University*, Blacksburg, VA, 1997.

[16] Lu Q. and Conners R., "A New Image Analysis Method for Automated Illicit Material Detection," *in Proceedings of the JCIS'98-Joint Conference on Information Science*, pp. 178-182, 1998.

[17] Lu Q. and Conners R., "X-ray Image Analysis for Luggage Detection," *in Proceedings of the 2nd Explosives Detection Technology Symposium and Aviation Security Technology Conference*, pp. 242-247, 1996.

[18] Manukian N., Wilensky G., Kirkwood J., and Chang J., "Neural Network Assisted Drug Detection in X-ray Images," *in Proceedings of International Conference on Neural Networks*, Houston, pp. 2497-2502, 1997.

[19] Murray N., Lacey R., and Mason P., "Exploitation of X-Ray Technology for the Detection of Contraband-Aviation Security Applications," *in Proceedings of European Conference on Security and Detection*, London, pp. 13-18, 1997.

[20] Perona P. and Malik J., "Scale-Space and Edge Detection using Anisotropic Diffusion," *IEEE Transactions on Pattern Analysis and Machine Intelligence*, vol. 12, no. 7, pp. 629-639, 1990.

[21] Pfeiffer F., Bech M., Bunk O., Kraft P., Eikenberry E., Brönnimann C., Grünzweig C., and David C., "Hard-X-ray Dark-field Imaging using a Grating Interferometer," *Nature Materials*, vol. 7, no. 2, pp. 134-137, 2008.

[22] Polski P., "International Aviation Security Research and Development," *Journal of* Testing *and Evaluation,* vol. 22, no. 3, pp. 267-274, 1994.

[23] Pramanik S., Zheng C., Zhang X., Emge T., and Li J., "New Microporous Metal-Organic Framework Demonstrating Unique Selectivity for Detection of High Explosives and Aromatic Compounds," *Journal of American Chemical Society*, vol. 133, no. 12, pp. 4153-4155, 2011.

[24] Qassim Q., Patel A., and Zin A., "Strategy to Reduce False Alarms in Intrusion Detection and Prevention Systems," *The International Arab Journal of Information Technology*, vol. 11, no. 5, pp. 500-506, 2014.

[25] Runkle R., White T., and Miller E., "Photon and Neutron Interrogation Techniques for Chemical Explosives Detection in Air Cargo: A Critical Review," *Nuclear Instruments and Methods in Physics Research*, vol. 603, no. 3 pp. 510-528, 2009.

[26] Singh S. and Singh M., "Explosives Detection Systems (EDS) for Aviation Security," *Signal Processing*, vol. 83, no. 1, pp. 31-55, 2003.

[27] Yang Y., Li T., and Li Y., "Explosives Detection Using Dual Energy X-ray Imaging and Photoneutron Analysis," *in Proceedings of IEEE Nuclear Science Symposium Conference*, Orlando, pp. 876-878, 2009.

Reza Hassanpour is affiliated with the Computer Engineering department of Cankaya University, Ankara-Turkey. He received his PhD in Computer Engineering from the Middle East Technical University, Ankara, Turkey in 2003. His main research interests are computer vision, pattern recognition and medical image processing.